Science
AAAS

Ultraviolet Imaging Spectroscopy Shows an Active Saturnian System

Larry W. Esposito, *et al.*

Science **307**, 1251 (2005);
DOI: 10.1126/science.1105606

7. R. F. Beebe, C. Barnet, P. V. Sada, A. S. Murrell, *Icarus* **95**, 163 (1992).
8. A. Sánchez-Lavega *et al.*, *Science* **271**, 631 (1996).
9. D. G. Andrews, J. R. Holton, C. B. Leovy, *Middle Atmosphere Dynamics* (Academic Press, New York, 1987), p.126.
10. B. J. Conrath, P. J. Gierasch, S. S. Leroy, *Icarus* **83**, 255 (1990).
11. B. Bézard, D. Gautier, *Icarus* **61**, 296 (1985).
12. B. J. Conrath, J. A. Pirraglia, *Icarus* **53**, 286 (1983).
13. B. Bézard, D. Gautier, B. Conrath, *Icarus* **60**, 274 (1984).
14. E. Anders, N. Grevesse, *Geochim. Cosmochim. Acta* **53**, 197 (1989).
15. M. H. Wong, P. R. Mahaffy, S. K. Atreya, H. B. Niemann, T. C. Owen, *Icarus* **171**, 153 (2004).
16. T. Owen, T. Encrenaz, *Space Sci. Rev.* **106**, 121 (2003).
17. H. Mizuno, *Prog. Theor. Phys.* **64**, 544 (1980).
18. J. B. Pollack *et al.*, *Icarus* **124**, 62 (1996).
19. R. Hanel *et al.*, *Science* **212**, 192 (1981).
20. R. Hanel *et al.*, *Science* **215**, 544 (1982).
21. L. Froidevaux, A. P. Ingersoll, *J. Geophys. Res.* **85**, 5929 (1980).
22. L. J. Spilker *et al.*, *Planet. Space Sci.* **51**, 929 (2003).
23. D. P. Simonelli *et al.*, *Icarus* **138**, 249 (1999).
24. J. R. Spencer, L. K. Tamppari, T. Z. Martin, L. D. Travis, *Science* **284**, 1514 (1999).
25. J. R. Spencer, thesis, University of Arizona, Tucson (1987).
26. J. A. Rathbun *et al.*, *Icarus* **169**, 127 (2004).
27. P. K. Seidelmann *et al.*, *Celest. Mech. Dynam. Astron.* **82**, 83 (2002).
28. A. Sánchez-Lavega, J. Rojas, P. Sada, *Icarus* **147**, 405 (2000).
29. L. W. Esposito, M. O'Callaghan, R. A. West, *Icarus* **56**, 439 (1983).
30. S. Albright, M. H. Elliott, and J. S. Tingley assisted with instrument commanding and data processing. D. Crick, M. de Cates, and S. Brooks assisted with observation designs. J. N. Cuzzi provided helpful comments on the manuscript. The authors acknowledge support from the NASA Cassini Project, the British Particle Physics and Astronomy Research Council, the Centre National d'Études Spatiales (CNES), and the Institut National des Sciences de l'Univers (CNRS/INSU).

Supporting Online Material
www.sciencemag.org/cgi/content/full/1105806/DC1
SOM Text
Figs. S1 and S2
Tables S1 and S2
References

29 September 2004; accepted 1 December 2004
Published online 23 December 2004;
10.1126/science.1105806
Include this information when citing this paper.

REPORT

Ultraviolet Imaging Spectroscopy Shows an Active Saturnian System

Larry W. Esposito,[1]* Joshua E. Colwell,[1] Kristopher Larsen,[1] William E. McClintock,[1] A. Ian F. Stewart,[1] Janet Tew Hallett,[2] Donald E. Shemansky,[2] Joseph M. Ajello,[3] Candice J. Hansen,[3] Amanda R. Hendrix,[3] Robert A. West,[3] H. Uwe Keller,[4] Axel Korth,[4] Wayne R. Pryor,[5] Ralf Reulke,[6] Yuk L. Yung[7]

Neutral oxygen in the saturnian system shows variability, and the total number of oxygen atoms peaks at 4×10^{34}. Saturn's aurora brightens in response to solar-wind forcing, and the auroral spectrum resembles Jupiter's. Phoebe's surface shows variable water-ice content, and the data indicate it originated in the outer solar system. Saturn's rings also show variable water abundance, with the purest ice in the outermost A ring. This radial variation is consistent with initially pure water ice bombarded by meteors, but smaller radial structures may indicate collisional transport and recent renewal events in the past 10^7 to 10^8 years.

The Cassini Ultraviolet Imaging Spectrograph (UVIS) (*1*) is part of the remote sensing payload of the NASA/European Space Agency (ESA) Cassini spacecraft. This spectrograph includes channels for extreme ultraviolet (EUV) and far ultraviolet (FUV) spectroscopic imaging, high-speed photometry of stellar occultations, solar EUV occultation, and a hydrogen/deuterium absorption cell (HDAC). UVIS science objectives are to study the composition, dynamics, and history of the saturnian system. UVIS extends the Voyager results of Broadfoot *et al*. in 1981 (*2*) and Sandel *et al*. in 1982 (*3*) through improved spectral and spatial resolution. We present results from the Saturn approach, systematic mosaics of the Saturn system, Phoebe, and Saturn Orbit Insertion (SOI). A highly structured and time-variable Saturn system is inferred from observations showing dynamic interactions between neutrals, ions, rings, moons, and meteoroids.

During the period preceding SOI, 25 December 2003 to 12 May 2004, spectral images of the saturnian system from the UVIS FUV and EUV spectrographs provided maps of the spatial distribution of emissions from neutral atomic hydrogen and oxygen. FUV mosaics of the Saturn system were obtained by stepping the slit position across the system in successive exposures of 200 s to 1000 s. Images in the atomic hydrogen Rydberg resonance transition at 121.57 nm (hydrogen Lyman-alpha) and the atomic oxygen resonance multiplet at 130.4 nm were obtained, both stimulated mainly in fluorescence of solar radiation. The observed oxygen has a full width at half maximum (FWHM) of ~4 Saturn radii (R_S) perpendicular to the orbital plane and ~16 R_S in the orbital plane (Fig. 1). Figure 1 is the second in the sequence of four images that follow the temporal variation of neutral oxygen. (The others are shown in figs. S1 to S4.) The figure shows a higher total abundance of oxygen that is more extensively distributed than in the previous and following images, which indicates that a transient event produced O in the Saturn system, followed by a rapid loss. The distribution of emission is asymmetric, with a peak near 3.7 R_S on the dark side of the planet. The total number of atomic oxygen atoms in this image is $> 4 \times 10^{34}$, or equivalent to 10^{12} g. Products of water dissociation, neutral oxygen, and OH [discovered in 1992 (*4*)] dominate the Saturn inner magnetosphere, in contrast to Jupiter, and H fills the entire magnetosphere, apparently extending through the magnetopause at far greater density than the ion population. The O and OH and a fraction of the H are products of water physical chemistry and derived ultimately from water ice.

The large abundance of neutrals limits the plasma abundance and electron temperature in the magnetosphere (*4*, *5*). The reactive system is self-limiting (*6*, *7*), because the ambient plasma ions are the source of neutral gas through reaction with E-ring grains. These, in turn, limit the plasma. With a water source, the system can achieve a quasi–steady state through the injection of energy supplied by hot electrons from the outer magnetospheric current system. One plausible source of water is collisions between larger, yet unseen parent bodies episodically resupplying water (*8*).

[1]University of Colorado, Laboratory for Atmospheric and Space Physics, 234 Innovation Drive, Boulder, CO 80303-7814, USA. [2]University of Southern California, 854 West 36th Place, Los Angeles, CA 90089–1191, USA. [3]Jet Propulsion Laboratory, 4800 Oak Grove Drive, Pasadena, CA 91109–8099, USA. [4]Max-Planck-Institut für Sonnensystemforschung, Max-Planck-Strasse 2, D-37191 Katlenburg-Lindau, Germany. [5]Central Arizona College, 8470 North Overfield Road, Coolidge, AZ 85228–9778, USA. [6]Stuttgart University, Institute for Photogrammetry, Geschwister-Scholl-Strasse 24-D, 70174 Stuttgart, Germany. [7]California Institute of Technology, Division of Geological and Planetary Sciences, 1200 East California Boulevard, Pasadena, CA 91125, USA.

*To whom correspondence should be addressed. E-mail: larry.esposito@lasp.colorado.edu

The inferred change in total oxygen mass in the magnetosphere over about a 2-month period is $\sim 5 \times 10^{11}$ g, equivalent to the total estimated mass in the micrometer-sized particle component of the E-ring system (*9*). Over a period of 100 million years, the loss rate inferred from these observations would consume the entire E-ring mass, even including postulated parent bodies.

The observed oxygen variation could result from a single injection of neutral gas, which then dissipated within about 2 months. This rapid loss cannot be explained by satellite sweeping, but charge capture from the plasma ions mixed with the neutrals has a calculated time scale for removal of the neutral gas comparable to the observations. (*6*, *7*). In the charge-capture process, a neutral O atom loses an electron to a resident plasma ion trapped by the magnetic field of Saturn in the region of the magnetosphere between 3 and 5 R_S. The main reactions are

$$O + O^+ \rightarrow O^+ + O \quad \text{(Reaction 1)}$$

$$O + OH^+ \rightarrow O^+ + OH \quad \text{(Reaction 2)}$$

$$O + H^+ \rightarrow O^+ + H \quad \text{(Reaction 3)}$$

Half of these reactions produce a neutralized ion with escape velocity. Reactions 1 to 3 thus remove neutral gas from the system into the interplanetary medium while replacing old ions with new ions. The neutral gas lost must be replaced from icy material in the source region (*4*, *5*). The mass loss rates calculated from the UVIS observations (*6*, *7*) are now 10 times as large as those derived by Shemansky *et al*. (*4*). Jurac *et al*. (*8*) concluded that ion sputtering of the icy satellites could not provide the required mass input and that only the larger surface area provided by the micron-sized ring particles could replace water molecules rapidly enough. This leaves open how gas is extracted from the ring particles and the generation of new particles to replace those converted into the gaseous state. Shemansky *et al*. (*6*, *7*) propose the formation of water cluster ions through adsorption of ambient plasma ions on the grains, with subsequent dissociative recombination into the vacuum, thus supplying the gas to the system. An example of one reaction is given here.

$$O^+ + G \rightarrow O_2H_2^+ \cdot (H_2O)_n \cdot G \quad \text{(Reaction 4)}$$

$$O_2H_2^+ \cdot (H_2O)_n \cdot G + e \rightarrow O_2 + H_2 + Gx \quad \text{(Reaction 5)}$$

Reaction 4 represents the formation of a cluster ion through adsorption of an O^+ ion onto a grain surface (G) in which $O_2H_2^+$ is formed in a stabilizing bond with a cluster of n H_2O molecules in the solid. Reaction 5 is a recombination reaction of the cluster ion with an ambient plasma electron resulting in the release of O_2 and H_2 molecules into the vacuum. Reactions like 4 and 5 have been measured in the laboratory (*8*) in the gas phase. Reaction 5 is known to be among the most rapid transitions in ion physics and reaction 4 is considered to be the rate-limiting factor (*7*). In summary, reactions 1 to 3 remove mass from the Saturn system but leave the number of ions in the plasma unchanged, and reactions such as 4 and 5 extract neutral gas from the icy grain population, replacing the lost neutrals and removing plasma from the volume. Balance requires the generation of new ice grains and energetic plasma ions to produce water molecules. We propose that the local ionization process and energy required to maintain this system is produced primarily from the injection of energetic electrons from the outer magnetosphere (*7*).

The UVIS data show that the neutral gas in the magnetosphere is subject to transient phenomena that insert large amounts of icy ring material into the central plasma and deposit a large amount of energy into the plasma. Our results emphasize the completely different states of the Jupiter and Saturn magnetospheres: Saturn's neutral/ion mixing ratio is 30,000 times greater. The energy-deposition rate in the Saturn inner magnetosphere that is required to maintain the state of the system in the 3 to 6 R_S region (*5*) is estimated at 1.4×10^{10} W. This energy is mainly consumed in removing mass from the system. Energy deposition in the Jupiter magnetosphere, 3×10^{12} W, is primarily invested in radiative loss.

Previous UV images of Saturn's H_2 and H emissions from the Hubble Space Telescope

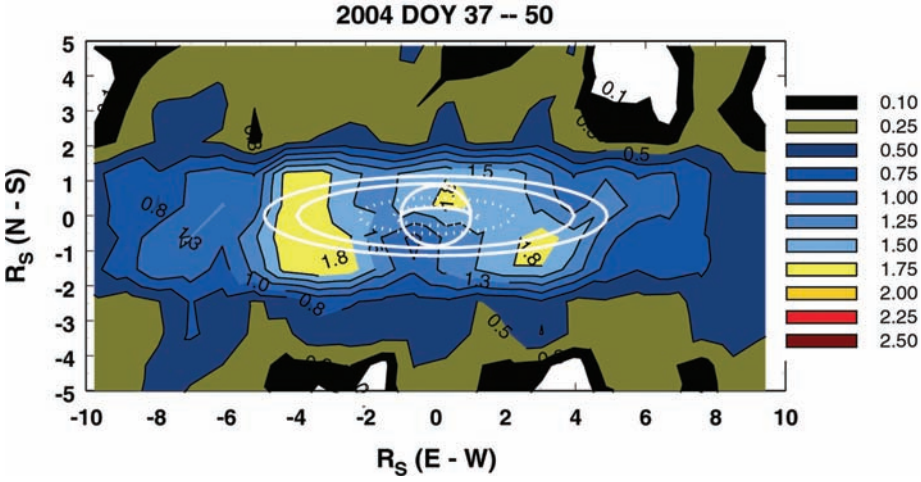

Fig. 1. The image of atomic oxygen emission from the Saturn system obtained in Cassini UVIS experiment observations from a range of 71 to 65 Mkm. The outline of the planet, orbits of Tethys, Enceladus (solid white lines), and outer A ring (dotted) are indicated. The subspacecraft point is at 13°4S latitude; solar radiation enters the system from the western side with a phase angle of 62° and a subsolar latitude of 23°S. The spatial resolution is 0.6 to 1.6 R_S. The image pixels are 0.9 × 0.9 R_S. North-south and east-west distances are indicated in R_S, with the origin at the center of the planet. Comparisons with UVIS observations made before and after this image show that it represents a much expanded emission distribution (figs. S1 to S4). Brightness values are in rayleighs. The expansion and subsequent decay of oxygen mass in the images show a characteristic time compatible with preliminary model calculations of charge-capture rates in the plasma.

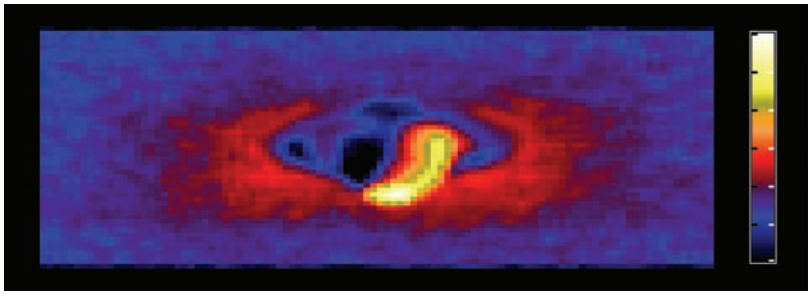

Fig. 2. Saturn's appearance in hydrogen Lyman-alpha. This image was acquired on 13 July 2004 from a range of 5 million km. Visible are the southern auroral zone, the sunlit crescent Saturn, the dark nightside, the dim rings, Saturn's shadow on the rings, and Saturn's extensive atomic hydrogen corona. The color bar is logarithmic, each tick representing a factor of 1.5 change in brightness.

(HST) show narrow auroral ovals in both the north and the south. These are probably due to primary electrons of 1 to 30 keV precipitating along the boundary of open and closed magnetic field lines (*10*). HST observed diurnal intensity variations of a factor of 10 and peak brightness near dawn, with evidence for auroral changes due to solar-wind variations (*11*–*13*). The UVIS image on 3 July 2004 (Fig. 2) shows strong UV polar aurora and dayglow emission at mid-latitudes. Magnetospheric neutral H also appears in an extended region near Saturn. The strongest emissions are from the south polar oval (~80° latitude). The north polar oval was tilted away from Cassini and appears only as polar limb emissions.

During July and August 2004, auroral emissions brightened episodically by up to a factor of 4. UVIS previously observed auroral brightenings at Jupiter due to solar-wind shock waves (*14*, *15*). A solar-wind shock wave on 25 July 2004 at 19:30 is followed by several days of enhanced solar-wind density in the Cassini Plasma Spectrometer (CAPS) data (*16*). This shock corresponds to the brightest UVIS-observed auroras so far. UVIS sees the two poles varying together. These Cassini UVIS and CAPS observations confirm that the solar wind perturbs Saturn's auroral emission.

Jupiter's spectrum from 2 January 2001 and Saturn's spectrum from 15 July 2004 are nearly identical spectrally (Fig. 3), showing H_2 band emissions from 115.0 to 170.0 nm (*17*). UVIS-derived hemispheric power input to Jupiter's auroral oval (10^{13} to 10^{14} W from electron precipitation) is about 200 times as large as that for Saturn's oval (10^{10} to 10^{11} W), in agreement with Voyager observations (*2*).

On 11 June 2004, as Cassini approached Saturn, the spacecraft flew by its outer moon, Phoebe. Distant observations of Phoebe were collected at a range of ≲380,000 km inbound and outbound, and mosaics were executed continuously through the closest approach at 2000 km. In addition, one full Phoebe rotation was monitored at 687,000 to 950,000 km. UVIS observed Phoebe in the EUV, FUV, and HDAC channels of the instrument.

The FUV spectrum (Fig. 4) was produced by averaging all pixels from the illuminated part of Phoebe during the mosaic taken near the closest approach (solar phase angle ~90°), divided by a solar spectrum obtained from the Solar Stellar Irradiation Comparison Experiment (SOLSTICE) (*18*) for the correct solar longitude. For comparison, the FUV reflectance spectrum of the Moon (similar solar phase angle) is also shown. The Phoebe spectrum displays a broad absorption feature centered near 160 nm, similar to that exhibited by H_2O frost and CO_2 frost (*19*, *20*). A model of Phoebe's reflectance spectrum combining H_2O frost, CO_2 frost, and a dark material to decrease the overall brightness is shown.

An FUV image of Phoebe obtained during the inbound portion of the flyby from a range of 31,300 km (Fig. 5) indicates that Phoebe is so dark that it blocks the Lyman-alpha emission of the Local Interstellar Medium (LISM), appearing silhouetted against the sky background. The heterogeneous surface reflectance shows brightness variations up to more than a factor of 2. These brightness variations are attributable to compositional variations (e.g., patchy ice distributions) across the surface, along with the rugged nature of Phoebe's surface, where steep slopes exposed to the sun appear brighter in this image.

As part of the investigation of Phoebe's origin, we searched for evidence of volatile emissions that would be indicative of comet-like activity such as that detected on Chiron. The set of long integrations acquired when Phoebe was ~1 pixel in size were summed to boost the potential signal level. The integrated spectrum showed no evidence of oxygen, carbon monoxide, or nitrogen emissions that would be anticipated if volatile activity were present. The 2σ upper limit for oxygen column density that UVIS could have detected given instrument sensitivity and the integration time is calculated to be $<2 \times 10^{13}$ cm^{-2} (*21*).

Phoebe has intrigued planetary scientists for decades because its great distance from Saturn (215 R_s) and Saturn's loose gravitational hold suggested that Phoebe was likely a captured object (*22*, *23*). Scientific curiosity has centered around the question of Phoebe's origin: Is it an errant asteroid or was it formed deep in the outer solar system? By detecting ice on Phoebe's surface, UVIS joins the other Cassini remote-sensing teams in concluding that Phoebe originated in the outer solar system.

During Cassini's orbit insertion on 30 June 2004, the spacecraft made its closest approach to Saturn's rings. During that period, the instrument slit was oriented roughly in the radial direction, and the detector was read out every 10 s, producing two approximately radial scans. During the scans, different parts of the detector sampled the same ring radius at different times as the spacecraft flew over the rings. We have summed all spectra from the same saturnocentric distance to provide a single spectral radial profile of the rings in the FUV. At any given radial position, about 60 spectra were recorded at sequential 10-s intervals, weighted by the amount of time spent and the fraction of the UVIS image pixel that is filled. Data were obtained in one scan for the outer C and inner B rings and in a

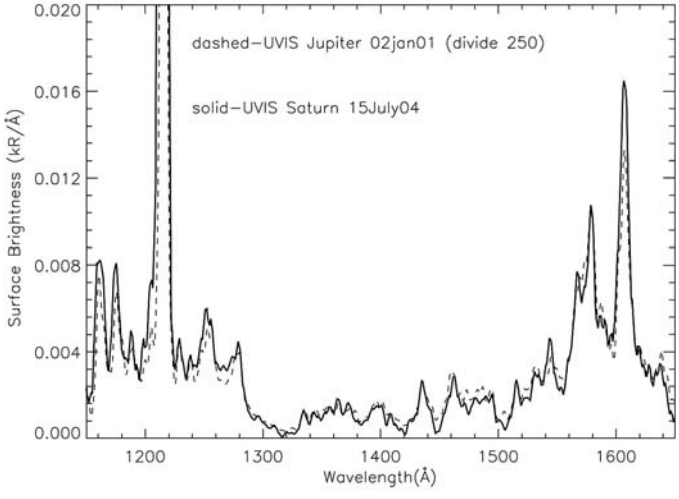

Fig. 3. Comparison of FUV spectra of Saturn (15 July 2004) and Jupiter (2 January 2001) southern auroral zones at ~0.5-nm resolution. Spectra are from a 28-min-duration system scan observation beginning at 03:38:22. Solar phase angle was near 90° for the dawn Saturn spectrum and 52° for the late afternoon Jupiter spectrum.

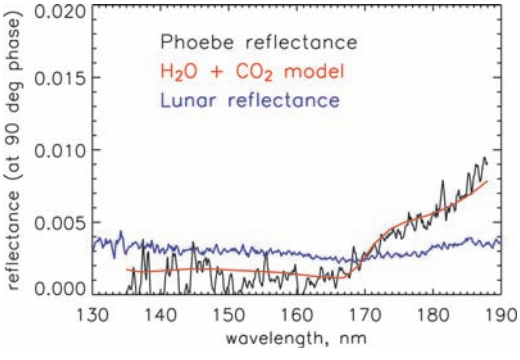

Fig. 4. Disk-averaged reflectance spectrum (obtained at 90° solar phase angle) of Phoebe compared with a model (red line), including laboratory spectra of H_2O frost and CO_2 frost (*20*). Also plotted is the UVIS-measured lunar FUV reflectance spectrum (blue line) for comparison. As a result of lower signal-to-noise ratios at wavelengths <150 nm, spectral features at the 3- to 6-nm scale may not be real.

second scan for the Cassini division and the A ring. Radial resolution is determined by the radial distance traversed by the footprint in the ring plane during each 10-s integration period, about 170 km in the first scan and 130 km in the second. To improve the photon-counting statistics, we adopted a resolution element of 150 km for both scans; this eliminates features that are below the noise level.

The ring brightness increases longward of 160 nm, consistent with absorption due to water ice at shorter wavelengths (*20*, *24*). At the shorter wavelengths, the ring signal is not distinguishable from the background except for the Lyman-alpha feature, which is a combination of scattered solar Lyman-alpha and Lyman-alpha from the local interstellar medium transmitted through the rings. Assuming that single scattering of sunlight dominates the observed brightness, which is a good approximation for this viewing geometry (*25*), we remove the geometric effects of the illumination and viewing angles and the optical depth to derive the product (AP) of the particle albedo, A, and the phase function, P (Fig. 6). In this approximation, fluctuations in AP indicate varying amounts of dark material mixed in with water ice. Without further observations, we cannot rule out more complex explanations of the fluctuations, for example, variations in vertical structure.

The A ring is the brightest ring region in the UV spectrum, the C ring is darkest, and the B ring is intermediate. The A-ring spectrum is similar to that of Phoebe (see Fig. 4), whereas the other rings are darker at long wavelengths, which indicates a lower fraction of water ice. In the A ring, the ice fraction, indicated in our data by UV reflectance longward of the water-ice absorption feature at 160 nm, increases outward to a maximum at the outer edge (Fig. 6). This large-scale variation is consistent with initially pure ice that has suffered meteoritic bombardment over the age of the solar system: The portions of Saturn's rings that have lower mass density become more polluted, and the subsequent transport of the darker material into the brighter rings over time explains the color gradients at the boundaries between rings (*26*).

We see variations over scales of 1000 to 3000 km in both ring scans that cannot be explained by this pollution mechanism operating over the age of the rings. These variations, which are not present in the Photopolarimeter Subsystem (PPS) optical depth profile, appear as small bumps and wiggles in the UVIS data in Fig. 6. Ballistic transport of spectrally neutral pollutants from meteoroids striking the rings produces broad gradients over this time period (*26*), too long to explain the finer structure in Fig. 6. We propose a class of smaller renewal events in which a small moon residing within the rings is shattered by an external impactor (*27*–*29*). We calculate the size of such a moon below. The interior of the moon has been shielded from external meteoritic bombardment and thus contains more pristine water ice. Because the amount of meteoroid pollution provides a rough clock to estimate the age of the rings (*26*), these random events reset that clock locally, making the material at that radial location younger and purer. As these purer ring particles collide with others, they interchange unconsolidated material on their surfaces, and the region of purer water-ice spectrum spreads radially, creating an ever-widening band of brighter material.

To estimate the time since such a reset event, we estimate the rate at which diffusion spreads the material. Using the kinematic viscosity $\nu \sim 280$ cm^2/s, the mass extinction coefficient $\kappa \sim 0.013$ cm^2/g (*30*, *31*), and the estimate of the fraction of regolith lost in a collision $f \sim 0.1$ (*32*), we calculate an effective diffusion coefficient for interchanging regolith material in the A ring

$$D_C \sim f * \nu \sim 30 \text{ cm}^2/\text{s}$$

Dimensional scaling gives an estimate of the time for such a renewal event to spread Δr = 1000 km as

$$T = \Delta r^2/D_C \sim 10^7 \text{year}$$

which is surely a lower estimate because f is uncertain. The mass needed to cover 10% of the surface area of average optical depth τ = 0.5, over an annulus Δr at saturnocentric distance r = 130,000 km is

$$M = 0.1 * 2\pi r\, \Delta r\, \tau/\kappa \sim 3 \times 10^{19} \text{g}$$

This mass is equivalent to a moon with radius $R \sim 20$ km.

Thus, the radial variations we interpret as due to differential pollution in our data set are consistent with the disruption of several small moons in the A ring in the past 10^7 to 10^8 years. This is one possible explanation of the variation in composition. Any process that releases pristine material, for example, the dredging of fresh material on ring particle surfaces by more energetic interparticle collisions at density wave locations, will create a brighter region in the rings. When the small moon Pan (*33*), $R \sim 10$ km, now residing in the nearby Encke gap, is eventually shattered by an external impact in the next 10 to 100 million years (*34*), our descendents will be treated to a spectacular sight: The gap will close up, and for some 10 to 100 million years thereafter a brighter radial swath of purer water ice at its former location will gradually spread and darken. Our interpretation of the spectral var-

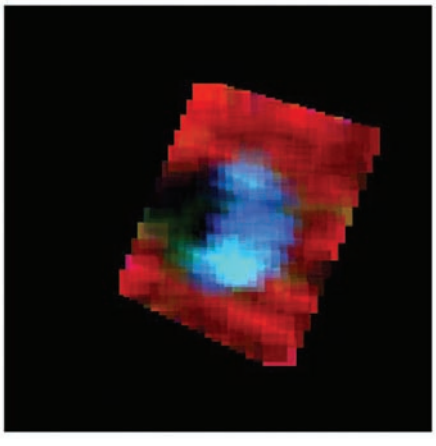

Fig. 5. FUV image of Phoebe, with solar illumination from the right. The red background corresponds to Lyman-alpha emission, blocked by Phoebe. Blue/green regions correspond to the longer FUV wavelengths (160 to 190 nm) and represent variability in brightness across the surface of Phoebe (up to a factor of more than 2 on the illuminated hemisphere).

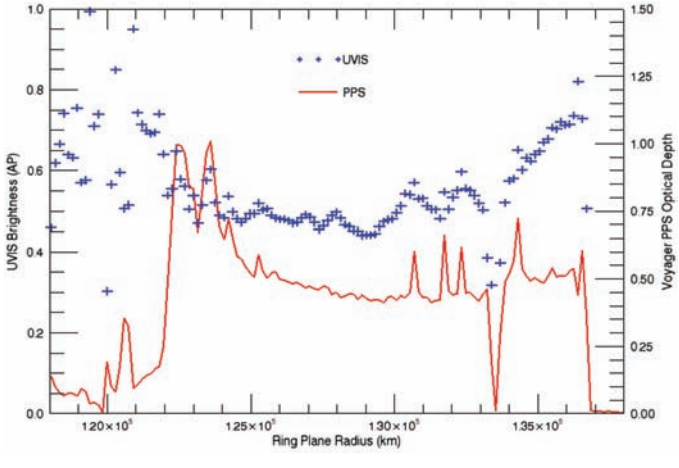

Fig. 6. The product of ring particle single-scattering albedo A, and particle phase function P, measured by UVIS, assuming that single scattering of sunlight dominates the measured brightness (blue). Absolute scale for AP is approximate. The Voyager PPS optical depth (red) shows the radial structure of the Cassini division (1.175 × 10^5 to 1.22 × 10^5 km) and the A ring. The UV brightness increases gradually toward the outer edge of the A ring with a sharp increase beyond the Encke gap at 1.335 × 10^5 km and a spike outside the Keeler gap at 1.365 × 10^5 km. Fluctuations at length scales of 1000 to 3000 km seen here and in the B ring indicate local variations in ring surface composition.

iations in Saturn's ring is thus consistent with a continual recycling of material between rings and moons, with the moons resupplying ring material when they are broken apart by collisions or meteorite impacts.

References and Notes

1. L. W. Esposito *et al.*, *Space Sci. Rev.*, in press.
2. A. L. Broadfoot *et al.*, *Science* **212**, 206 (1981).
3. B. Sandel *et al.*, *Science* **215**, 548 (1982).
4. D. E. Shemansky, P. Matheson, D. T. Hall, H.-Y. Hu, T. M. Tripp, *Nature* **363**, 329 (1993).
5. D. E. Shemansky, D. T. Hall, *J. Geophys. Res.* **97**, 4143 (1992).
6. D. E. Shemansky, Cassini UVIS team, paper presented at meeting of Committee on Space Research, Paris, France, 18 July 2004.
7. D. E. Shemansky *et al.*, in preparation.
8. S. R. Jurac, R. E. Johnson, J. D. Richardson, *Icarus* **149**, 384 (2001).
9. A. Juhasz, M. Horanyi, *J. Geophys. Res.* **107**, 1066 (2002).
10. J. T. Trauger *et al.*, *J. Geophys. Res.* **103**, 20237 (1998).
11. S. W. H. Cowley, E. J. Bunce, R. Prange, *Ann. Geophysicae* **22**, 1379 (2004).
12. J. C. Gerard *et al.*, *J. Geophys. Res.* **109**, A09207 (2004).
13. R. Prange *et al.*, *Nature*, in press.
14. D. A. Gurnett *et al.*, *Nature* **415**, 985 (2002).
15. W. R. Pryor *et al.*, in preparation.
16. D. T. Young *et al.*, *Science* **307**, 1262 (2005).
17. C. Jonin, X. Liu, J. M. Ajello, G. James, H. Abgrall, *Astrophys. J. Suppl.* **129**, 247 (2000).
18. W. E. McClintock, G. J. Rottman, T. N. Woods, *SPIE Proc.* **4135**, 225 (2000).
19. S. G. Warren, *Appl. Optics* **25**, 2650 (1986).
20. J. K. Wagner, B. W. Hapke, E. N. Wells, *Icarus* **69**, 14 (1987).
21. The gas detection threshold is based on a minimum 2σ detectable level of 10 counts above background, instrument sensitivity at 130.4 nm of 3.4 cts/kR-s, integration time of ~0 hours, and solar-wind values for the electron density and temperature at Saturn.
22. M. Cuk, J. A. Burns, *Icarus* **167**, 369 (2004).
23. J. B. Pollack, J. A. Burns, M. E. Tauber, *Icarus* **37**, 587 (1979).
24. R. Wagener, J. Caldwell, *ESA Special Publication SP-281* **1**, 85 (1988).
25. L. Dones, J. N. Cuzzi, M. R. Showalter, *Icarus* **105**, 184 (1993).
26. J. N. Cuzzi, P. R. Estrada, *Icarus* **132**, 1 (1998).
27. J. E. Colwell, L. W. Esposito, *J. Geophys. Res.* **98**, 7387 (1993).
28. J. M. Barbara, L. W. Esposito, *Icarus* **160**, 161 (2002).
29. L. W. Esposito, J. E. Colwell, paper presented at meeting of American Geophysical Union, San Francisco, CA, 8 December 2003.
30. L. W. Esposito, M. O. Callaghan, R. A. West, *Icarus* **56**, 439 (1983).
31. L. W. Esposito, *Icarus* **67**, 345 (1986).
32. R. M. Canup, L. W. Esposito, *Icarus* **119**, 427 (1996).
33. M. R. Showalter, *Nature* **351**, 709 (1991).
34. J. E. Colwell, L. W. Esposito, D. Bundy, *J. Geophys. Res.* **105**, 17589 (2000).

35. Thanks to H. Tollerud for assistance with data processing, L. Bloom for producing the manuscript, and J. Cuzzi and the anonymous reviewers for helpful comments. This work is one part of the Cassini UVIS investigation, supported by the NASA Jet Propulsion Laboratory Cassini mission.

Supporting Online Material

www.sciencemag.org/cgi/content/full/1105606/DC1
Figs. S1 to S4

23 September 2004; accepted 2 December 2004
Published online 16 December 2004;
10.1126/science.1105606
Include this information when citing this paper.

REPORT

Radio and Plasma Wave Observations at Saturn from Cassini's Approach and First Orbit

D. A. Gurnett,[1]* W. S. Kurth,[1] G. B. Hospodarsky,[1] A. M. Persoon,[1] T. F. Averkamp,[1] B. Cecconi,[1] A. Lecacheux,[2] P. Zarka,[2] P. Canu,[3] N. Cornilleau-Wehrlin,[3] P. Galopeau,[3] A. Roux,[3] C. Harvey,[4] P. Louarn,[4] R. Bostrom,[5] G. Gustafsson,[5] J.-E. Wahlund,[5] M. D. Desch,[6] W. M. Farrell,[6] M. L. Kaiser,[6] K. Goetz,[7] P. J. Kellogg,[7] G. Fischer,[8] H.-P. Ladreiter,[8] H. Rucker,[8] H. Alleyne,[9] A. Pedersen[10]

We report data from the Cassini radio and plasma wave instrument during the approach and first orbit at Saturn. During the approach, radio emissions from Saturn showed that the radio rotation period is now 10 hours 45 minutes 45 ± 36 seconds, about 6 minutes longer than measured by Voyager in 1980 to 1981. In addition, many intense impulsive radio signals were detected from Saturn lightning during the approach and first orbit. Some of these have been linked to storm systems observed by the Cassini imaging instrument. Within the magnetosphere, whistler-mode auroral hiss emissions were observed near the rings, suggesting that a strong electrodynamic interaction is occurring in or near the rings.

Magnetized planets such as Saturn have many complicated radio and plasma wave phenomena. Here we present the first results from the Cassini Radio and Plasma Wave Science (RPWS) instrument (*1*) during the approach and first orbit around Saturn. The RPWS instrument is designed to measure the electric and magnetic fields of radio emissions and plasma waves across a broad range of frequencies, from 1 Hz to 16 MHz for electric fields and from 1 Hz to 12 kHz for magnetic fields. A Langmuir probe is also included to measure the density and temperature of the local plasma. Our observations are organized in the order in which the data were obtained, starting with radio emissions detected during the approach to Saturn, continuing through the region near the closest approach, and ending ~3 months after orbital insertion.

The Voyager 1 and 2 spacecraft first established that Saturn is an intense radio emitter. The primary component of this radiation is called Saturn kilometric radiation (SKR), because the peak intensities occur in the kilometer wavelength range (*2*), typically at frequencies from ~100 to 400 kHz. Just as with the other giant planets, the intensity of this radio emission is modulated by the rotation of the planet. During the Voyager flybys of Saturn in 1980 to 1981, the SKR modulation period was found to be 10 hours 39 min 24 ± 7 s (*3*). Because the charged particles responsible for the radio emission are controlled by the magnetic field, which is linked to the deep interior of the planet, and because the planet has no visible surface, this period has been widely adopted as the rotation period of Saturn (*4*). However, measurements by the Ulysses spacecraft (*5*) have shown that the radio rotation period is not constant.

This variability has now been confirmed by the Cassini observations. The RPWS first began to detect SKR in early April 2002, at a radial distance of ~2.5 astronomical units (AU) from Saturn. As the spacecraft approached Saturn, the signal strength gradually increased to the point that an accurate measurement of the SKR modulation period could be obtained. A normalized power spectrum of the fluctuations in the SKR intensity (Fig. 1) shows a sharp peak at a period of 10 hours 45 min 45 ± 36 s. Compared with the Voyager spectrum (Fig. 1), it

[1]Department of Physics and Astronomy, University of Iowa, Iowa City, IA 52242, USA. [2]Observatoire de Paris, 92195 Meudon, France. [3]Centre d'Etude des Environments Terrestre et Planétaires (CETP)–L'Institut Pierre-Simon La Place, 78140 Velizy, France. [4]Centre d'Etude Spatiale des Rayonnements–CNRS, 31028 Toulouse, France. [5]Swedish Institute of Space Physics, SE-751 21 Uppsala, Sweden. [6]NASA Goddard Space Flight Center, Greenbelt, MD 20771, USA. [7]Department of Physics and Astronomy, University of Minnesota, Minneapolis, MN 55455, USA. [8]Austrian Academy of Sciences, Space Research Institute, A-8042 Graz, Austria. [9]Department of Automatic Control and Systems Engineering, University of Sheffield, Sheffield S1 4DU, UK. [10]Department of Physics, University of Oslo, Blindern, N-0316 Oslo, Norway.

*To whom correspondence should be addressed. E-mail: donald-gurnett@uiowa.edu

ERRATUM

Post date 3 June 2005

Special Section: Cassini at Saturn: Reports: "Ultraviolet imaging spectroscopy shows an active saturnian system" by L. W. Esposito *et al.* (25 Feb. 2005, p. 1251). On page 1252, in the third column, in the paragraph after reactions 4 and 5, line 10, the citation of reference 8 is incorrect. The citation should be to the following paper, which is not in the reference list: M. T. Leu, M. A. Biondi, R. Johnsen, *Phys. Rev. A* **7**, 292 (1973).